

Fine-Tuning Hybrid Physics-Informed Neural Networks for Vehicle Dynamics Model Estimation

Shiming Fang, *Student Member, IEEE*, and Kaiyan Yu, *Member, IEEE*

Abstract—Accurate dynamic modeling is critical for autonomous racing vehicles, especially during high-speed and agile maneuvers where precise motion prediction is essential for safety. Traditional parameter estimation methods face limitations such as reliance on initial guesses, labor-intensive fitting procedures, and complex testing setups. On the other hand, purely data-driven machine learning methods struggle to capture inherent physical constraints and typically require large datasets for optimal performance. To address these challenges, this paper introduces the Fine-Tuning Hybrid Dynamics (FTHD) method, which integrates supervised and unsupervised Physics-Informed Neural Networks (PINNs), combining physics-based modeling with data-driven techniques. FTHD fine-tunes a pre-trained Deep Dynamics Model (DDM) using a smaller training dataset, delivering superior performance compared to state-of-the-art methods such as the Deep Pacejka Model (DPM) and outperforming the original DDM. Furthermore, an Extended Kalman Filter (EKF) is embedded within FTHD (EKF-FTHD) to effectively manage noisy real-world data, ensuring accurate denoising while preserving the vehicle’s essential physical characteristics. The proposed FTHD framework is validated through scaled simulations using the BayesRace Physics-based Simulator and full-scale real-world experiments from the Indy Autonomous Challenge. Results demonstrate that the hybrid approach significantly improves parameter estimation accuracy, even with reduced data, and outperforms existing models. EKF-FTHD enhances robustness by denoising real-world data while maintaining physical insights, representing a notable advancement in vehicle dynamics modeling for high-speed autonomous racing.

Index Terms—Physical-informed neural network, vehicle dynamics, Extended Kalman Filter, model estimation

I. INTRODUCTION

ACCURATE vehicle dynamics modeling is essential for the development of algorithms that enable effective control of autonomous vehicles, particularly in high-speed and agile driving scenarios. These models enable precise prediction and response to real-world driving conditions, which is critical for ensuring safety during rapid vehicle maneuvers. While kinematic models provide a simpler approach by focusing on geometric parameters, they fail to capture key dynamic aspects such as tire forces, suspension behavior, throttle response, and drivetrain effects. This highlights the importance of dynamic models, which delve deeper into the vehicle performance and allow for the estimation of longitudinal and lateral forces to

better predict vehicle motion. A key challenge in dynamic modeling is the estimation of sensitive coefficients in tire models, such as the Pacejka coefficients [1], which can be both complex and time-consuming to estimate accurately.

Traditional methods for estimating tire models come with several limitations, including reliance on initial guesses, long fitting times, and challenges associated with testing setups. Deep neural networks (DNNs) have been employed to handle the non-linearity in vehicle dynamics modeling [2], offering a simpler solution that bypasses the requirement for specialized testing equipment. Yet, purely data-driven machine learning approaches often fail to capture the underlying physical constraints of the system and are highly dependent on large datasets. Moreover, these models can produce outputs that do not reflect the real system dynamics.

To address these shortcomings, Physics-Informed Neural Networks (PINNs) have been proposed. PINNs incorporate governing equations and physical laws into neural network architectures, improving both model efficiency and accuracy, while requiring less data. Despite these advantages, PINNs still depend on high-quality, low-noise data. This has led researchers to explore techniques such as data augmentation, transfer learning, and novel data collection strategies. PINNs have been shown to be effective in various scientific domains, including fluid dynamics and structural mechanics. In the context of autonomous driving, methods like the Deep Pacejka Model (DPM) [3] and Deep Dynamics Model (DDM) [4] have been applied to high-speed racing scenarios. However, these models have limitations. For instance, DPM relies heavily on sampling-based control and unconstrained parameter estimation, with tests only conducted in simulation environments. While DDM offers improvements by constraining estimation ranges, it still struggles with smaller datasets and noisy data during training [4].

While supervised PINNs (which rely on input data to reveal physical laws) require large datasets, unsupervised PINNs (which leverage governing equations directly) and hybrid approaches require fewer labeled data points. Building on this, we propose the Fine-Tuning Hybrid Dynamics (FTHD) method, which, to the best of our knowledge, is the first to use a fine-tuning hybrid PINN model to estimate vehicle dynamics. Furthermore, we introduce the Extended Kalman Filter FTHD (EKF-FTHD), the first model to incorporate an embedded EKF to denoise real-world data while maintaining physical insights. The major contributions of this paper are as follows:

- 1) We present FTHD, a fine-tuned hybrid PINN method designed to estimate key vehicle parameters, including Pacejka tire coefficients, drivetrain coefficients, and mo-

An earlier version of this paper will be presented in part at the 2024 Modeling, Estimation, and Control Conference, Chicago, Illinois, USA, in October 27–30, 2024. (*Corresponding author: Kaiyan Yu*).

S. Fang and K. Yu are with the Department of Mechanical Engineering, Binghamton University, Binghamton, NY 13902 USA (email: sfang10@binghamton.edu; kyu@binghamton.edu).

Source codes are available at <https://github.com/Binghamton-ACSR-Lab/FTHD>.

ment of inertia. Compared to the state-of-the-art methods, FTHD achieves higher accuracy while requiring smaller datasets.

- 2) We introduce EKF-FTHD, a data processing method that embeds an EKF within the FTHD framework. This approach denoises real-world data by separating the noise from the physical signal, providing more accurate predictions. Compared to traditional smoothing methods and recent PINN models, EKF-FTHD demonstrates superior performance in revealing physical insights from noisy data, with reduced loss and improved prediction accuracy during further training.

Building upon our previous conference publication [5], which introduced the FTHD method based on the ideal simulation data for scaled vehicles, this journal paper extends the work by proposing EKF-FTHD model to handle real-world experimental data. EKF-FTHD functions as a data-processing model that filters and denoises noisy, real-world data while retaining essential physical characteristics, allowing FTHD to achieve more accurate parameter estimation and a lower validation loss. This improvement directly addresses the limitations of previous models in managing noisy datasets. In addition, this journal paper provides further experimental results and more detailed analyses, demonstrating that the hybrid approach, even with smaller training datasets, significantly improves parameter estimation in real-world conditions. This advancement marks a major step forward in vehicle dynamics modeling for high-speed autonomous racing.

The rest of the paper is organized as follows: In Section II, we discuss existing methods for vehicle dynamics modeling, their limitations, and recent advancements. Section III outlines the problem statement and provides an overview of the vehicle model, the proposed FTHD model, and the EKF-FTHD pre-processing method for handling noisy data. The experimental results are presented in Section IV, where the performance of the FTHD and EKF-FTHD models is evaluated. Finally, the concluding remarks are summarized in Section V, highlighting the key contributions and future directions.

II. RELATED WORK

Vehicle dynamics modeling for autonomous driving has been extensively studied, with models ranging from simple point mass representations to more complex single-track (bicycle) dynamic models (STMs) and multi-body systems. The choice of model often depends on the complexity of the driving scenario. For low-speed, non-slip conditions, kinematic models are typically used as they focus on geometric aspects. However, these models struggle to represent more complex driving conditions, especially during high-speed maneuvers where dynamic factors such as tire forces and vehicle inertia become critical. While the bicycle model strikes a balance between simplicity and accuracy in high-speed and drifting scenarios, maintaining accurate parameter estimation for this model remains a challenge [6]. Several data-driven methods have been proposed to estimate vehicle model parameters. For example, [7] introduced a data-driven approach for identifying longitudinal dynamics, and [8] explored homotopy optimization for parameter identification in dynamic systems modeled

by ordinary differential equations. However, these methods often assume simplified conditions like low speeds and time-invariant parameters, which are inadequate for the high-speed, time-dependent dynamics seen in autonomous racing, as highlighted in [4]. Alternative approaches, such as those presented by [9] and [10], apply Gaussian Processes Regression to account for model uncertainties and enhance prediction accuracy. While these methods capture time-dependent physics, they may not always guarantee predictions that satisfy physical constraints.

The estimation of parameters for tire models, such as the widely-used Pacejka Magic Formula [1], is inherently non-linear. Recent advancements using deep neural networks have shown promise in capturing these non-linearities, especially in autonomous racing [2]. While DNNs reduce the complexity and costs of traditional parameter estimation methods, they still require large datasets for training and often fail to capture the underlying physical laws. Furthermore, purely data-driven models, such as those described in [11] and [12], struggle to generalize to scenarios beyond the data they were trained on and can produce outputs that are not physically meaningful. In an effort to address these challenges, [13] used a Gated Recurrent Unit (GRU)-structured neural network to potentially replace traditional physics-based STMs in simulating autonomous racing vehicles. While this approach yields more accurate predictions of vehicle dynamics within the training data, it still encounters difficulties in predicting conditions beyond the scope of the training data.

The growing interest in revealing physical laws has led to increasing research into PINNs, which combine data-driven models with the ability to uncover underlying physical laws [14]. For example, recent work in the field of autonomous driving, such as [15], implements an online-adjusted method to estimate cornering stiffness in real-time. However, their approach assumes a linear relationship between slip angles and forces, which restricts its applicability in handling non-linear regions, especially at large slip angles. This limitation becomes critical in high-speed autonomous racing scenarios involving significant drifting. Other recent studies, such as DPM [3] and DDM [4], focus on estimating the magic formula using PINN-based models. However, DPM relies on sampling-based control and exhibits unconstrained Pacejka coefficient estimations, which reduces its effectiveness [4]. In contrast, DDM has demonstrated improved performance over DPM by producing results within reasonable ranges, but it suffers from a lack of robustness when trained on smaller datasets. While DDM offers both open-loop and closed-loop performance, it incorporates Model Predictive Control (MPC) for trajectory optimization. As a result, it becomes difficult to evaluate the accuracy of the estimated magic formula parameters because the control is optimized within the MPC process. Additionally, as shown in [4], when handling real-world data collected from sensors, the inherent noise from measurements introduces significant challenges. This noise leads to high losses, oscillations in the predicted states, and difficulties in model convergence, thereby obscuring the true underlying physical insights. Traditional data pre-processing methods, such as the low-pass Savitzky-Golay filter [16], can smooth the noisy data,

but as curve-fitting methods, they fail to adequately reveal the physical insights, resulting in persistently high losses.

To overcome these challenges, we introduce FTGD, a novel hybrid approach that integrates PINN-based fine-tuning with enhanced noise-handling capabilities. FTGD is designed to reduce the required dataset size and improve parameter estimation by separating noise from the data, leading to more accurate predictions. To the best of our knowledge, this is the first model that employs hybrid techniques for fine-tuning vehicle dynamics modeling in high-speed autonomous racing environments. Fine-tuning, a widely used technique in machine learning, involves adapting a pre-trained model to a related task. This approach is commonly utilized across fields such as Natural Language Processing and Computer Vision, demonstrating its versatility and effectiveness.

To further address the challenges posed by noisy data in dynamic modeling, we extended the design of the guard layer from DDM and FTGD by incorporating an EKF guard layer. This layer leverages the EKF's ability to estimate the state and predict errors in non-linear systems [17]. The proposed EKF-enhanced FTGD, EKF-FTGD, aims to separate noisy data into two distinct components: a physical part that reflects the underlying vehicle dynamics and a noise part that can be discarded in further training. By doing so, the EKF-FTGD ensures that the physical insights of the vehicle dynamics are retained, leading to improved model accuracy.

In terms of data collection for dynamic model parameter estimation, various platforms can be utilized, including full-sized and scaled autonomous racing competitions like the Indy Autonomous Challenge [18] and F1tenth [19]. Simulators such as BayesRace [9], which use predefined vehicle models with MPC to generate state data, are also widely employed. These platforms provide essential datasets for training and testing the models proposed in this work.

III. PROBLEM STATEMENT

A. Vehicle Dynamics

In this paper, we employ the STM, also known as the bicycle dynamic model. The STM simplifies the four-wheel structure into a two-wheel bicycle structure by assuming that the slip angles for the wheels on a particular axle are the same, effectively combining all wheels on one axle into a single wheel in the middle, as depicted in Fig. 1. The state and input variables of the model are outlined in Table I.

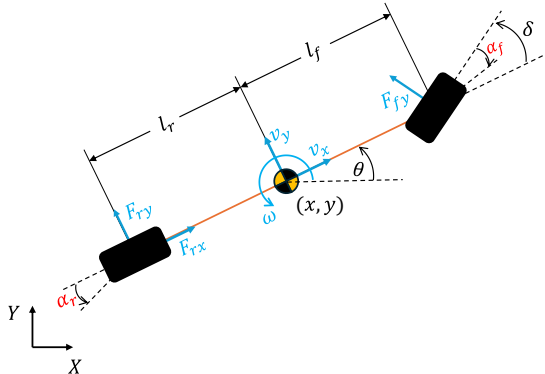


Fig. 1. A schematic of the STM configuration.

TABLE I
NOTATION FOR STATE AND INPUT VARIABLES

Variables	Notation
Horizontal Position (m)	x
Vertical Position (m)	y
Inertial Heading (rad)	θ
Longitudinal Velocity (m/s)	v_x
Lateral Velocity (m/s)	v_y
Yaw Rate (rad/s)	ω
Throttle (%)	\mathcal{T}
Steering Angle (rad)	δ
Change in Throttle (%)	$\Delta\mathcal{T}$
Change in Steering Angle (rad)	$\Delta\delta$

As reported in [9], the longitudinal force at the rear wheel is determined by:

$$F_{rx} = (C_{m1} - C_{m2}v_x^2)\mathcal{T} - C_{r0} - C_dv_x^2. \quad (1)$$

C_{m1} and C_{m2} represent drivetrain coefficients, with C_{m1} (N) linearly related to throttle and C_{m2} (kg/s) related to damping. C_{r0} (N) and C_d (kg/m) denote the rolling resistance and the drag resistance, respectively. This simplifies the drag and rolling resistance forces as $F_d = C_dv_x^2$ and $F_{r0} = C_{r0}$. According to the Pacejka tire model, the slip angles α_f and α_r can be calculated as

$$\begin{aligned} \alpha_f &= \delta - \arctan\left(\frac{\omega l_f + v_y}{v_x}\right) + S_{hf}, \\ \alpha_r &= \arctan\left(\frac{\omega l_r - v_y}{v_x}\right) + S_{hr}, \end{aligned}$$

where S_{hf} and S_{hr} represent the horizontal shift of the front and rear slip angles, respectively. Let S_{vf} and S_{vr} represent the vertical shift of the front and rear lateral forces. The lateral forces are given by $F_{fy} = S_{vf} + D_f \sin(C_f \arctan(B_f \alpha_f - E_f(B_f \alpha_f - \arctan(B_f \alpha_f))))$ at the front wheel and $F_{ry} = S_{vr} + D_r \sin(C_r \arctan(B_r \alpha_r - E_r(B_r \alpha_r - \arctan(B_r \alpha_r))))$ at the rear wheel. Here, $B_i, C_i, D_i, E_i, i = f, r$ are the remaining Pacejka coefficients [20]. l_f and l_r denote the distances from the vehicle's center of mass to the front and rear axles, respectively. At time t , the system states are represented by $\mathbf{S}_t = [x_t, y_t, \theta_t, v_{x_t}, v_{y_t}, \omega_t, \mathcal{T}_t, \delta_t] \in \mathbb{R}^8$, and the control inputs U_t include changes in throttle and steering: $U_t = [\Delta\mathcal{T}_t, \Delta\delta_t]^T \in \mathbb{R}^2$. The state equation can be obtained as follows:

$$\begin{aligned} x_{t+1} &= x_t + (v_{x_t} \cos \theta_t - v_{y_t} \sin \theta_t) \Delta t, \\ y_{t+1} &= y_t + (v_{x_t} \sin \theta_t + v_{y_t} \cos \theta_t) \Delta t, \\ \theta_{t+1} &= \theta_t + (\omega_t) \Delta t, \\ v_{x_{t+1}} &= v_{x_t} + \frac{1}{m} (F_{rx} - F_{fy} \sin \delta_t + m v_{y_t} \omega_t) \Delta t, \\ v_{y_{t+1}} &= v_{y_t} + \frac{1}{m} (F_{ry} + F_{fy} \cos \delta_t - m v_{x_t} \omega_t) \Delta t, \\ \omega_{t+1} &= \omega_t + \frac{1}{I_z} (F_{fy} l_f \cos \delta_t - F_{ry} l_r) \Delta t, \\ \mathcal{T}_{t+1} &= \mathcal{T}_t + \Delta\mathcal{T}, \quad \delta_{t+1} = \delta_t + \Delta\delta, \end{aligned} \quad (2)$$

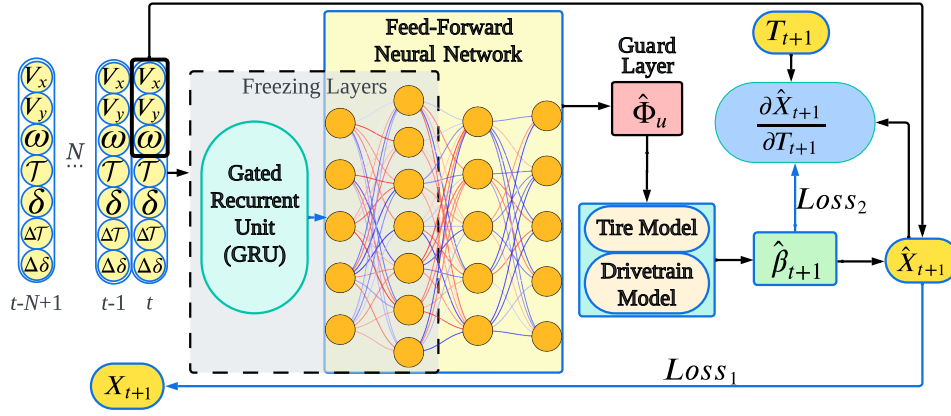


Fig. 2. The structure of the proposed FTHD PINN model involves freezing layers of the pre-trained DDM and using a hybrid unsupervised loss for fine-tuning.

where m denotes the mass of the vehicle, I_z represents the moment of inertia, and Δt is the time step between the next time step and the current time step.

To estimate the vehicle dynamics, similar to DDM, we categorize all coefficients of the model into two groups: $\Phi_k = [l_r, l_f, m]$, which are readily available or easy to measure, and $\Phi_u = [B_i, C_i, D_i, E_i, S_{hi}, S_{vi}, C_{m1}, C_{m2}, C_{r0}, C_d, I_z]$, where $i = f, r$, which are more challenging to measure directly and will be estimated by the model. Let $\Phi = \Phi_k \cup \Phi_u$. This paper employs a hybrid method to fine-tune the DDM, assuming that each estimated coefficient falls within a predefined nominal range $\underline{\Phi}_u \leq \Phi_u \leq \bar{\Phi}_u$, where $\underline{\Phi}_u$ and $\bar{\Phi}_u$ represent the lower and upper bounds, respectively. Additionally, the modeling approach assumes certain conditions: the vehicle operates on a 2D surface, disregarding the influence of the z-axis; any delay in the action commands is neglected, i.e., the inputs are applied to the model without any delays.

B. FTHD PINN Model

In the proposed FTHD model, similar to the models defined by DDM [4] and DPM [3], with the given $X_t = [v_{x_t}, v_{y_t}, \omega_t, T_t, \delta_t] \in \mathbb{R}^5$ and $U_t = [\Delta T, \Delta \delta] \in \mathbb{R}^2$, the evolution of the position states x_t, y_t, θ_t can be calculated using Eq. (2).

During the pre-training phase, like DDM, FTHD collects N continuous time steps ($N \geq 1$) as the input $\mathbf{X}_{\text{input}} = [X_{t-N+1}, \dots, X_t]$ from the training dataset. Subsequently, it predicts the estimated state $\hat{X}_{t+1} = [\hat{v}_{x_{t+1}}, \hat{v}_{y_{t+1}}, \hat{\omega}_{t+1}]$ at time $t+1$, which is then compared with the label $X_{t+1} = [v_{x_{t+1}}, v_{y_{t+1}}, \omega_{t+1}]$ using Mean-Square-Error (MSE) loss for backpropagation:

$$Loss_1 = \text{MSE}(\hat{X}_{t+1}, X_{t+1}).$$

After the pre-training phase, the entire state dictionary, denoted as $\Theta = \{W, b\}$, is selected for the hybrid fine-tuning process. Here, W and b represent the weights and biases of the model, respectively. During the fine-tuning process, we selectively freeze n layers of the model, where n is determined based on the total number of hidden layers in the architecture. Importantly, we ensure that at least one hidden

layer (excluding activation layers) remains active and unfrozen to allow for continued learning and adaptation. The number of frozen layers n is chosen to balance stability and adaptability during the fine-tuning phase, ensuring the model can still adjust to new data while preserving key features learned during pre-training. The gradients of the frozen parameters, denoted as $\Theta_f = \{W_f, b_f\}$, are no longer updated, while only the active parameters, $\Theta_a = \{W_a, b_a\}$, participate in backpropagation. This strategy allows the model to retain the knowledge captured in the frozen layers while adapting the active layers to the new data, improving performance with a smaller training dataset. This process is illustrated in Fig. 2.

Compared to the DDM, the training dataset for the proposed model includes an additional time input, T_{t+1} alongside X_t and U_t , resulting in a structured dataset $\mathbf{D} = [[X_1, U_1, T_2], \dots, [X_N, U_N, T_{N+1}]]$. This augmentation is inspired by the time constraint loss in physically constrained neural networks introduced by [21], where a time partial differential equation (PDE) serves as one of the unsupervised loss functions. In the domain of autonomous driving, this approach is relevant due to the relationship between velocity derivatives and acceleration, as inferred from the model's output:

$$\hat{X}_{t+1} = [\hat{v}_{x_{t+1}}, \hat{v}_{y_{t+1}}, \hat{\omega}_{t+1}] = f(X_t, U_t, \Phi_k, \Phi_u, T_{t+1}).$$

Using input time T_{t+1} and the intermediate estimated acceleration $\hat{\beta}_{t+1} = [a_{x_{t+1}}, a_{y_{t+1}}, \dot{\omega}_{t+1}]$, the unsupervised loss is defined as:

$$Loss_2 = \text{MSE} \left(\frac{\partial \hat{X}_{t+1}}{\partial T_{t+1}}, \hat{\beta}_{t+1} \right).$$

$Loss_2$ serves as an unsupervised loss that is unrelated to the label X_{t+1} . This loss function aims to ensure that, given the input X_t and assuming the time interval Δt is small enough, the model outputs an estimated \hat{X}_{t+1} such that the difference $\hat{X}_{t+1} - \hat{X}_t$ is close to the estimated acceleration $\hat{\beta}$. Without providing the label, the estimated \hat{X}_{t+1} could vary freely, but it still satisfies the dynamic motion constraints.

Following the approach of [22] and [21], when handling the hybrid loss of the model, two weights, w_1 and w_2 , are introduced, where $w_1 + w_2 = 1$. In this framework, $Loss_1$

is prioritized to ensure the fine-tuned model effectively aligns with the dynamics of a specific vehicle, as it is directly related to vehicle-specific characteristics. On the other hand, $Loss_2$ serves to generalize the model, ensuring that the derivative of local longitudinal and lateral speeds corresponds to the longitudinal and lateral accelerations, thereby refining the underlying physics. By incorporating $Loss_2$, the model parameters receive additional curvature updates after the DDM, allowing for improved convergence towards a shared local minimum, even when the dataset size is reduced. This approach ensures that the model retains both specific vehicle dynamics and generalizable physical insights, optimizing performance with limited data. The total loss of the model, $Loss_{total}$, is then calculated as a weighted sum of $Loss_1$ and $Loss_2$, expressed as:

$$Loss_{total} = w_1 \cdot Loss_1 + w_2 \cdot Loss_2. \quad (3)$$

Eq. (3) combines the supervised loss $Loss_1$ (driven by the training labels and the model outputs) with the unsupervised loss $Loss_2$ (driven by the PDE constraints of the model's internal features, without relying on labels). This approach assumes that when the loss driven by labeled data is sufficiently low but struggles to further decrease the validation error, integrating the unsupervised loss provides additional constraints to the model, allowing for more opportunities for the model's state to update. By using this hybrid method with adaptive weights, which combines supervised and unsupervised learning, it becomes possible to train the model with less data while still achieving higher accuracy compared to using solely supervised PINNs.

We incorporate the physics guard layer, designed for DDM, which proves beneficial as it restricts the output Pacejka coefficients within a predefined nominal boundary $[\Phi_u, \bar{\Phi}_u]$, ensuring that the resulting relationships between lateral force and slip angle are always physically consistent. This is achieved through: $\hat{\Phi}_u = \sigma(z) \cdot (\bar{\Phi}_u - \Phi_u) + \Phi_u$, where z represents the elements in the last hidden layer, constrained by the size of Φ_u . These are then passed through sigmoid activation layers and scaled by a preset range to yield the estimated $\hat{\Phi}_u$.

However, unlike the pure-data driven DNN, the prediction \hat{X}_{t+1} is derived from the input state and the estimated Pacejka coefficients based on the STM vehicle dynamics and Eq. (2), the convergence of $Loss_1$ may be influenced by the backpropagation of the guard layer. Even though the guard layer ensures that the estimated Pacejka coefficients fall within the range, it can still be challenging for the model to find the optimal states that satisfy all drifting conditions. This challenge can be attributed to the local minima problem, as discussed in [23], which demonstrates that a sigmoid-based neural network can lead to suboptimal local minima. Since the guard layer of DDM employs a sigmoid function and outputs each of the Pacejka coefficients independently, if one of them reaches a local minimum, the sigmoid function may struggle to further update it. These local minimum coefficients can then influence other coefficients, especially when they are combined in the tire model and the drivetrain model in Eq. (1), particularly as the slip angle increases and the force relationship becomes nonlinear [1]. Moreover, when the size of the training dataset

is reduced, if one or more Pacejka coefficients reach local minima, the entire model may converge to a local minimum, making it challenging to further reduce the loss if no new data is added to the training process.

Therefore, the proposed FTHD utilizes a fine-tuning model and unsupervised method to address this issue. If the model is reaching or approaching a local minimum, freezing some layers and adding new loss functions to the loss space could help update coefficients whose gradients do not change. The use of a hybrid method could further reduce the training dataset while maintaining accuracy compared to supervised-only PINNs.

C. EKF-FTHD Pre-Processing Method

As discussed in DDM [4], when processing data collected from real-world scenarios like the Indy Autonomous Challenge, noise poses a significant challenge for achieving convergence comparable to simulation-based models. This is largely due to sensor-based data, which relies on physical measurements rather than computed values. As a result, the real data often exhibits oscillations, even when the car operates at nearly stable speeds. These oscillations introduce noise, degrading the model's performance. While traditional smoothing methods, such as the Savitzky-Golay filter [16], can improve convergence by smoothing the data, they overlook the physical relationships between variables such as X_t and U_t , potentially leading to feature loss and residual errors.

To address this, we propose the EKF-FTHD pre-processing method, which leverages EKF's ability to estimate states in nonlinear systems. Table II summarizes the variables used in the proposed method. Here, \hat{X}_{t+1} represents the estimated state output by the model, while X_{t+1} denotes the measurements obtained from the sensor at the time step $t + 1$.

TABLE II
NOTATION FOR VARIABLES USED IN THE EKF-FTHD MODEL

Variables	Notation
Model state vector at time $t + 1$	\hat{X}_{t+1}
Filtered state vector at time $t + 1$	$\hat{X}_{\text{EKF},t+1}$
Measurement at time $t + 1$	X_{t+1}
Nonlinear state transition function	$f(\cdot)$
Nonlinear measurement function	$h(\cdot)$
Jacobian of f w.r.t. X_{t+1}	F_{t+1}
Jacobian of h w.r.t. \hat{X}_{t+1}	H_{t+1}
Covariance matrix at time $t + 1$	P_{t+1}
Process noise covariance	Q_{t+1}
Measurement noise covariance	R_{t+1}

Based on the FTHD model shown in Fig. 2, we incorporate an EKF guard layer embedded with a covariance matrix to denoise the raw state $X_{t+1} = [v_{x_{t+1}}, v_{y_{t+1}}, \omega_{t+1}]$, splitting it into a physical component and a noise component: $X_{t+1} = X_{\text{EKF},t+1} \cup \epsilon$. The estimated parameters include $\Phi_{\text{EKF}} = \Phi_u \cup \Phi_f$, where $\Phi_f = [q_j, r_j]$ and $j = v_x, v_y, \omega$. Each coefficient is assumed to lie within a nominal range: $\underline{\Phi}_f \leq \Phi_f \leq \bar{\Phi}_f$, with $\underline{\Phi}_f$ and $\bar{\Phi}_f$ represent the lower and

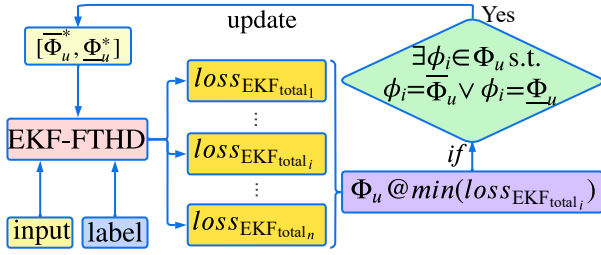


Fig. 4. Illustration of the process for updating the preset coefficient ranges using the EKF-FTHD method.

By integrating the EKF within the FTTHD model and adjusting the noise covariance matrices, the EKF-FTHD effectively separates the data into physical and noise components, which contrasts with the DDM approach. The separated physical part $X_{\text{EKF}_{t+1}}$ decreases the impact of noise and focuses more on the vehicle's dynamics. Furthermore, the range of the estimated parameters significantly influences the training process. Specifically, smaller ranges tend to yield better convergence. However, without access to the ground truth of real data, determining the optimal range is challenging. Due to the oscillatory nature of the parameters, even if the preset ranges do not align with the true values, the DDM may still estimate an intermediate value within the specified range. This introduces ambiguity in assessing whether the result from DDM is indeed the best estimate. Our experiments indicate that with the original DDM preset range $[\bar{\Phi}_u, \bar{\Phi}_u^*]$ the model outputs coefficients that hit the boundary of the range. By adjusting the range to $[\Phi_u^*, \bar{\Phi}_u^*]$, both DDM and EKF-FTHD achieve smaller loss values and better convergence. Fig. 4 shows the process of updating the preset coefficient ranges, where ϕ_i represents each parameter of Φ_u defined in Section III-A.

After completing EKF-FTHD training, using hyperparameter tuning similar to that in the FTTHD process, we select the model with the lowest loss. This pre-process model, along with the corresponding X_{EKF_t} , is used as the new dataset, with adjusted coefficient ranges $[\Phi_u^*, \bar{\Phi}_u^*]$. To validate the effectiveness of this dataset and the adjusted ranges, we train the FTTHD model following a similar simulation process with X_{EKF_t} and $[\Phi_u^*, \bar{\Phi}_u^*]$ as the dataset and coefficients ranges, demonstrating the EKF-FTHD method's advantages in data processing and coefficient adjustment. We also compare the DDM model trained with X_{EKF_t} and the adjusted range $[\Phi_u^*, \bar{\Phi}_u^*]$ to the original DDM from [4]. Results and discussions are presented in the next section.

IV. RESULT AND DISCUSSION

A. Training Dataset

We compare the simulation performance of the proposed FTTHD against the state-of-the-art DDM, using data collected from the simulator described in [9]. This simulator features a 1:43 scaled racecar engaged in pure-pursuit of a reference trajectory on the racetrack depicted in Fig. 5. The ground truth (GT) of the scaled racecar's coefficients is available but only used for comparison after training. The sampling frequency is 50 Hz, resulting in a time interval between samples Δt_{sim} is

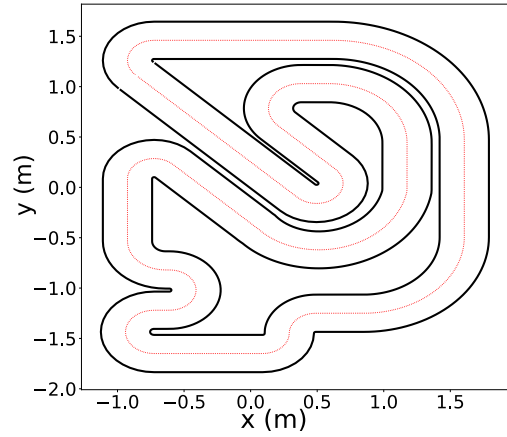


Fig. 5. The racetrack utilized for data collection.

0.02 s. The total size of the simulation dataset $\mathbb{D}_{\text{total}}^{\text{sim}}$ consists of 1000 samples.

To further evaluate the real-world performance of the FTTHD model and compare it with DDM in terms of the accuracy of the filtered data and adjusted parameter ranges derived from EKF-FTHD, we use a real-world dataset from a full-scale Indy autonomous racecar [24]. The dataset includes fused measurements from two RTK-corrected GNSS signals and an IMU, which are passed through a 100 Hz EKF. The sampling frequency of the real data is 25 Hz, resulting in a time interval between samples of $\Delta t_{\text{exp}} = 0.04$ s. The total dataset size, denoted as $\mathbb{D}_{\text{total}}^{\text{exp}}$, consists of 11,488 samples collected at the Putnam Park Road Course in Indianapolis. The EKF-FTHD filters the full dataset, $\mathbb{D}_{\text{total}}^{\text{exp}}$, and output a new dataset, denoted as $\mathbb{D}_{\text{total}}^{\text{EKF}}$, which is then used to train both the FTTHD and DDM models for prediction.

To demonstrate the robustness of our method compared to DDM when reducing the training dataset size, we simulate random selections of 30%, 20% and 15% of the dataset samples $\mathbb{D}_{\text{train}}^{\text{sim}}$ for training, with $\mathbb{D}_{\text{total}}^{\text{sim}}$ used for validation. For real-world experiments, we randomly select 90%, 60%, 30%, 15% and 5% of the dataset samples for training, denoted as $\mathbb{D}_{\text{train}}^{\text{exp}}$ and $\mathbb{D}_{\text{train}}^{\text{EKF}}$. The full datasets $\mathbb{D}_{\text{total}}^{\text{exp}}$ and $\mathbb{D}_{\text{total}}^{\text{EKF}}$ are used for validation. Both models undergo the same number of training iterations, using identical hyperparameter tuning to minimize validation loss.

B. Model Coefficient Ranges

To estimate the physics coefficient values $\hat{\Phi}_u$ in the physics guard layer of the model, as shown in Fig. 3, as well as the estimated EKF covariance values $\hat{\Phi}_f$, the bounds $\bar{\Phi}_u$ and $\bar{\Phi}_u^*$, as well as $\bar{\Phi}_f$ and $\bar{\Phi}_f^*$, are required. For simulation experiments, we use the known GT to compare the performance of FTTHD with DDM, using the same coefficient ranges as in [4]. In real-world experiments, the bounds $[\bar{\Phi}_u, \bar{\Phi}_u^*]$ used in [4] are adjusted to $[\Phi_u^*, \bar{\Phi}_u^*]$ based on EKF-FTHD output. The covariance bounds $[\bar{\Phi}_f, \bar{\Phi}_f^*]$ are set according to the quality of the raw data, where better-quality data lead to smaller covariance values. These ranges are detailed in Table III, and Table IV provides the EKF covariance matrix ranges.

TABLE III
COEFFICIENT RANGES FOR THE DYNAMIC STM

Layers	Coefficient	Sim $[\Phi_u, \bar{\Phi}_u]$		Real $[\Phi_u, \bar{\Phi}_u]$		Real $[\Phi_u^*, \bar{\Phi}_u^*]$	
		Front	Rear	Front	Rear	Front	Rear
Pacejka Layer	B	[5.0, 30.0]	[5.0, 30.0]	[5.0, 30.0]	[5.0, 30.0]	[1.0, 20.0]	[1.0, 20.0]
	C	[0.5, 2.0]	[0.5, 2.0]	[0.5, 2.0]	[0.5, 2.0]	[0.1, 1.5]	[0.1, 1.5]
	D	[0.1, 1.9]	[0.1, 1.9]	[100, 10 ⁴]	[100, 10 ⁴]	[10, 8 × 10 ³]	[10, 8 × 10 ³]
	E	[-2.0, 0.0]	[-2.0, 0.0]	[-2.0, 0.0]	[-2.0, 0.0]	[-2.0, 5.0]	[-2.0, 10.0]
	S_v	[-0.003, 0.003]	[-0.003, 0.003]	[-300, 300]	[-300, 300]	$[-2 \times 10^3, 300]$	$[-2 \times 10^3, 300]$
	S_h	[-0.02, 0.02]	[-0.02, 0.02]	[-0.02, 0.02]	[-0.02, 0.02]	[-0.02, 0.2]	[-0.02, 0.2]
Drivetrain Layer	C_{m1} (N)	[0.1435, 0.574]		$[500, 2 \times 10^3]$		$[100, 1 \times 10^4]$	
	C_{m2} (kg/s)	[0.0273, 0.109]		[0, 1.0]		[0, 5.0]	
	C_{r0} (N)	[0.0259, 0.1036]		[0.1, 1.4]		[0.1, 1.4]	
	C_d (kg/m)	$[1.75 \times 10^{-4}, 0.1036]$		[0.1, 1.4]		[0.1, 1.4]	
Inertia Layer	I_z (kg·m ²)	$[1.39 \times 10^{-5}, 5.56 \times 10^{-5}]$		$[5 \times 10^5, 2 \times 10^3]$		$[5 \times 10^3, 2 \times 10^4]$	

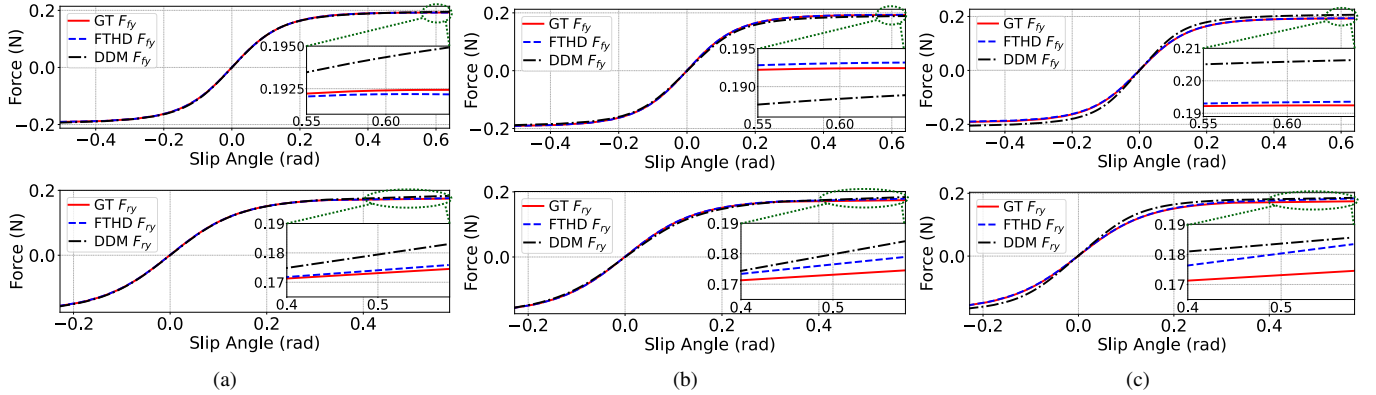


Fig. 6. Comparison of the front wheel lateral force F_{fy} (top) and the rear wheel lateral force F_{ry} (bottom) using the trained coefficients with the proposed FTHD scheme, DDM model, and the GT. The force responses of the trained coefficients using (a) 30%, (b) 20%, and (c) 15% of the total training set. (inset) Zoomed-in comparison.

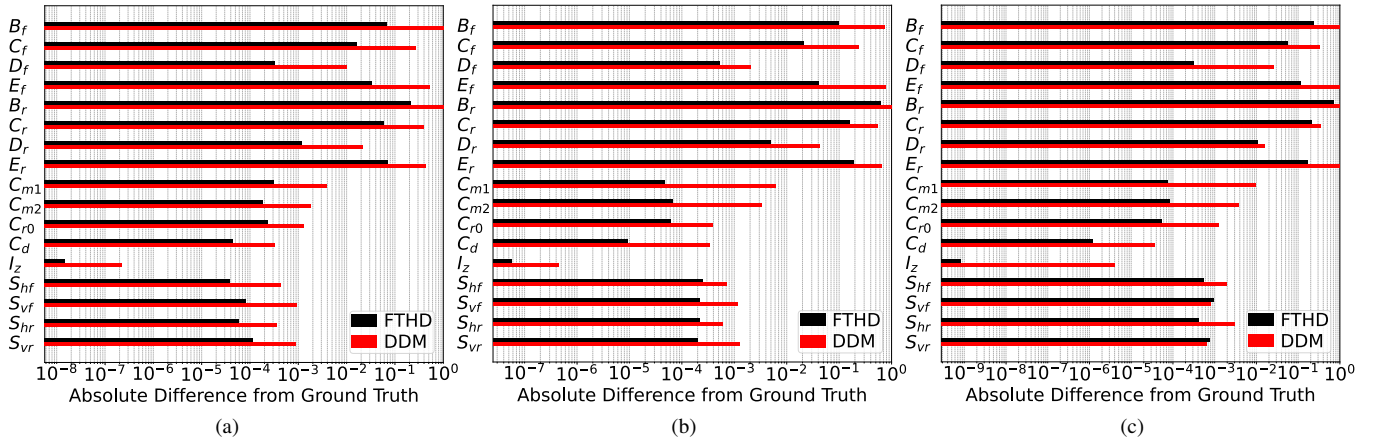


Fig. 7. Absolute difference between FTHD and DDM estimated Pacejka, Drivetrain and moment of inertia coefficients compared to the GT using (a) 30%, (b) 20%, and (c) 15% of the total training set.

C. Evaluation Metrics

For the simulation, with known GT, we use the Pacejka and drivetrain coefficients that result in the lowest validation loss from both FTHD and DDM to calculate lateral forces using the same STM. During the fine-tuning hybrid training of FTHD, we choose weight parameters $w_1 = 0.99975$ and $w_2 = 0.00025$. The comparison results with the GT are shown in Fig. 6. It's evident that as the size of the training set decreases, the FTHD retains better alignment with the GT

outputs compared to DDM. Furthermore, it's clear to see that when only 15% of the training set is used, the force plots of DDM show much greater deviation from the GT, while FTHD can still closely approximate it.

To evaluate the estimation performance of FTHD and DDM in simulation, we compare the minimum validation loss, $L_{\min} = \min(Loss_{\text{val}})$, the root-mean-square-error (RMSE) of velocities, and the maximum errors of velocities (ϵ_{\max}) for v_x , v_y and ω , as used in [4]. Additionally, we evaluate

TABLE IV
COEFFICIENT RANGES OF THE COVARIANCE MATRICES FOR THE
EKF-FTHD MODEL

Layer	Coefficient	Real Data	
		Min	Max
EKF Layer	q_{v_x}	0.1	1
	q_{v_y}	0.1	1
	q_ω	0.1	1
	r_{v_x}	0.01	1.0
	r_{v_y}	0.01	1.0
	r_ω	1×10^{-4}	0.01

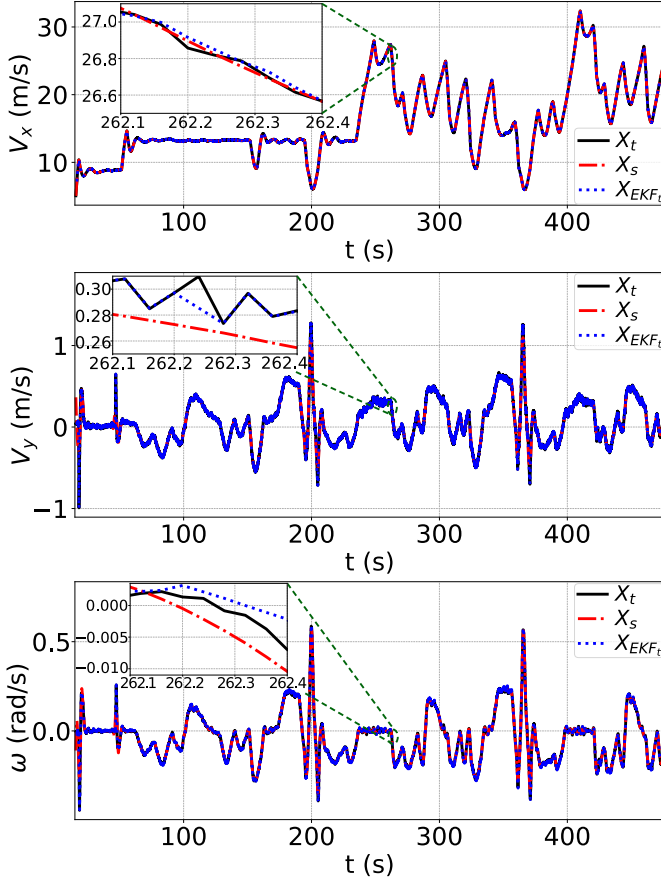


Fig. 8. Comparison of raw data, traditionally smoothed data, and EKF-filtered data in the real-world dataset. (inset) Zoomed-in comparison.

the absolute difference between the parameters estimated by FTHD and DDM from the GT, using datasets reduced to 30%, 20% and 15% of the total sample data. The results, shown in Table VI and Fig. 7 reveal that even with the same number of iterations (15k in total) for both models during training, the FTHD outperforms the supervised-only PINN. The estimated Pacejka coefficients also exhibit less difference with the GT. Additionally, even when the dataset is reduced, the FTHD maintains significantly higher accuracy in estimating the moment of inertia I_z compared to DDM.

In the real-world experiments, we use \mathbb{D}^{EKF} for training the FTHD model. Fig. 8 presents the plots of v_x , v_y and ω over time, where X_t refers to the raw data from $\mathbb{D}^{\text{total}}$, X_s represents the traditionally smoothed data, and X_{EKF_t} corresponds to the data from \mathbb{D}^{EKF} . Upon comparison, it is clear that although X_s

TABLE V
VALIDATION LOSS COMPARISON OF DDM TRAINED ON ORIGINAL
DATASET AND EKF DATASET, WITH PRESET AND EKF-FTHD ADJUSTED
PARAMETER RANGES, ACROSS VARYING TRAINING DATA RATIOS

$\mathbb{D}^{\text{train}}_{\text{train}}^{\text{exp}}$ or $\mathbb{D}^{\text{train}}_{\text{EKF}}$	$\mathbb{D}^{\text{total}}_{\text{total}}^{\text{exp}}$ with $[\Phi_u, \bar{\Phi}_u]$	\mathbb{D}^{EKF} with $[\Phi_u^*, \bar{\Phi}_u^*]$
90%	1.480×10^{-4}	7.004×10^{-5}
60%	2.132×10^{-4}	1.235×10^{-4}
30%	2.922×10^{-4}	1.894×10^{-4}
15%	3.290×10^{-4}	2.220×10^{-4}
5%	3.859×10^{-4}	2.854×10^{-4}

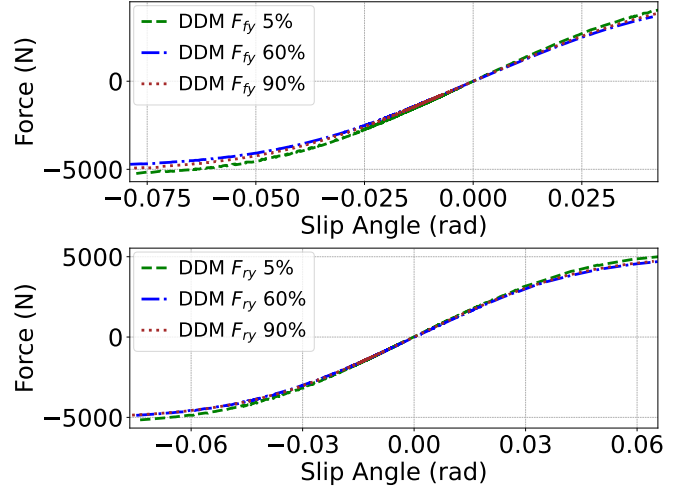


Fig. 9. Lateral force response of the DDM model in real-world experiments as the size of the training set decreases.

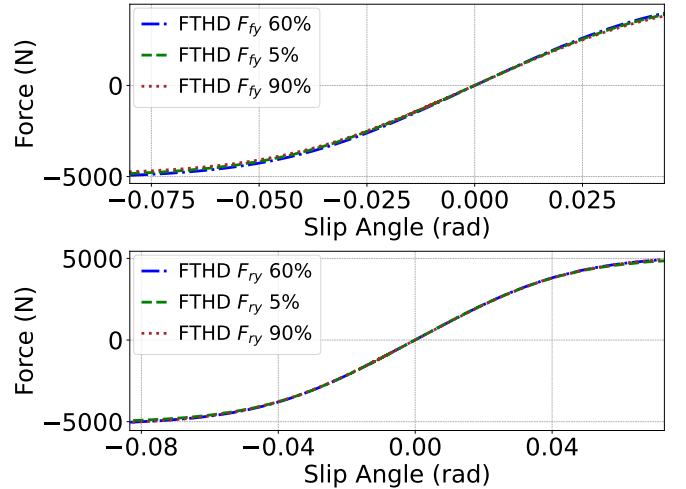


Fig. 10. Lateral force response of the FTHD model in real-world experiments as the size of the training set decreases.

smooths the data, it results in a loss of key features and alters the relationship between the states and controls. In contrast, X_{EKF_t} separates noise from X_t while preserving the physically meaningful aspects of the data.

To demonstrate the improvement in data fidelity after the EKF-FTHD processing, we train DDM models on both $\mathbb{D}^{\text{total}}$ and \mathbb{D}^{EKF} , with preset parameter ranges $[\Phi_u, \bar{\Phi}_u]$ and EKF-

FTHD adjusted ranges $[\bar{\Phi}_u^*, \bar{\Phi}_u^*]$. The validation losses, presented in Table V, show that with the same structured model, the filtered dataset \mathbb{D}^{EKF} achieves higher accuracy across different training data ratios.

Since the GT for vehicle parameters is unknown in real-world experiments, it becomes difficult to assess the model’s quality solely based on force plots. Additionally, due to variations in the dynamic coefficients of the vehicle over time, such as tire wear and changing road conditions, it is challenging to describe all situations using a single set of parameters. To better illustrate this issue, rather than relying on a constant tire model, we present the dynamic force and velocity responses for both the FTHD and DDM models. Fig. 9 and Fig. 10 depict the force response as the training dataset size decreases from 90% to 5%. Fig. 9 shows the DDM model trained and tested using data from $\mathbb{D}_{\text{total}}^{\text{exp}}$, while Fig. 10 displays the FTHD model trained and tested with data from \mathbb{D}^{EKF} . As the training set size decreases, the DDM’s force plot deviates significantly at larger slip angles, whereas the FTHD model maintains a more consistent result, even with only 5% of the training data - closely resembling the plot from 90%. Fig. 11 and Fig. 12 show the velocity predictions of DDM and FTHD for real-world data. The FTHD predictions exhibit smaller errors compared to the GT velocities. Table VII compares the minimum validation loss (L_{\min}), the RMSE for velocities, and the maximum velocity errors (ϵ_{\max}) for v_x , v_y , and ω , for different training data ratios from $\mathbb{D}_{\text{total}}^{\text{exp}}$ and \mathbb{D}^{EKF} . Even with the same number of training iterations (2k in total) for both models, the FTHD model consistently outperforms the supervised-only PINN DDM in predicting v_x and v_y , with the prediction of ω showing only minor differences. Notably, even as the training set size decreases to 5%, the FTHD model maintains more accuracy than DDM.

D. Hyperparameters Tuning

To ensure a fair comparison without the influence of model hyperparameters, we utilize Tune [25] and set up identical configuration spaces and trials for both models. This includes the selection of hidden layers, GRU layers, neurons, learning rate, the choice of N for each input features $\mathbf{X}_{\text{input}}$, and batch size, as well as the frozen layers during fine-tuning process. To simplify the process of hyperparameters selection, we set the size of frozen layers equal to the 3/4 of the total layers for each tests. Both models are trained on the same hardware: a GeForce RTX 4090 GPU, a 13th Gen Intel Core i7-13700K CPU, and 128 GB of RAM. To further challenge the model’s performance, the full training set is used for validation. The lowest validation loss and the corresponding Φ are used for the simulation comparisons. In the real experiment, we use the EKF-FTHD model with the lowest validation loss to generate the filtered dataset used for training the FTHD estimation model, then select the hyperparameter configuration with the lowest validation loss for dynamical performance comparisons. Tables VIII and IX show the model configurations where the lowest validation loss occurs after reducing the training dataset size. In the simulations, each configuration represents both DDM and FTHD with the same original dataset. In the real

TABLE VI
COMPARISON OF RMSE, VALIDATION LOSS, AND MAXIMUM VELOCITY ERRORS FOR FTHD AND DDM IN SIMULATION EXPERIMENTS ACROSS DIFFERENT TRAINING SET SIZES

$\frac{\mathbb{D}_{\text{train}}^{\text{sim}}}{\mathbb{D}_{\text{total}}^{\text{sim}}}$		DDM		FTHD	
		RMSE	ϵ_{\max}	RMSE	ϵ_{\max}
80%	v_x	6.70×10^{-6}	2.83×10^{-5}	5.96×10^{-6}	1.53×10^{-5}
	v_y	1.96×10^{-5}	3.61×10^{-5}	3.07×10^{-6}	1.22×10^{-5}
	ω	8.19×10^{-5}	5.07×10^{-4}	3.82×10^{-5}	2.30×10^{-4}
	L_{\min}	2.38×10^{-9}		5.01×10^{-10}	
50%	v_x	2.49×10^{-5}	6.63×10^{-5}	1.70×10^{-5}	1.18×10^{-5}
	v_y	1.51×10^{-5}	5.34×10^{-5}	1.68×10^{-5}	3.35×10^{-5}
	ω	1.44×10^{-4}	1.32×10^{-3}	4.83×10^{-5}	2.89×10^{-4}
	L_{\min}	7.15×10^{-9}		9.68×10^{-10}	
30%	v_x	3.76×10^{-5}	1.50×10^{-4}	7.46×10^{-6}	2.07×10^{-5}
	v_y	8.61×10^{-5}	4.84×10^{-4}	2.30×10^{-5}	7.33×10^{-5}
	ω	8.66×10^{-4}	1.79×10^{-2}	1.02×10^{-4}	6.16×10^{-4}
	L_{\min}	2.53×10^{-7}		3.67×10^{-9}	
20%	v_x	1.16×10^{-5}	8.60×10^{-5}	1.14×10^{-5}	5.03×10^{-5}
	v_y	8.46×10^{-5}	3.69×10^{-4}	1.50×10^{-5}	5.33×10^{-5}
	ω	6.48×10^{-4}	6.52×10^{-3}	1.29×10^{-4}	1.22×10^{-3}
	L_{\min}	1.42×10^{-7}		5.68×10^{-9}	
15%	v_x	8.60×10^{-5}	3.50×10^{-4}	4.25×10^{-5}	2.35×10^{-4}
	v_y	4.99×10^{-4}	1.48×10^{-3}	1.38×10^{-4}	6.68×10^{-4}
	ω	1.54×10^{-3}	1.35×10^{-2}	4.22×10^{-4}	2.92×10^{-3}
	L_{\min}	8.74×10^{-7}		6.64×10^{-8}	

TABLE VII
COMPARISON OF RMSE, VALIDATION LOSS, AND MAXIMUM VELOCITY ERRORS FOR FTHD AND DDM IN REAL-WORLD EXPERIMENTS ACROSS DIFFERENT TRAINING SET SIZES

Training Set Ratio		DDM ($\mathbb{D}_{\text{total}}^{\text{exp}}$)		FTHD (\mathbb{D}^{EKF})	
		RMSE	ϵ_{\max}	RMSE	ϵ_{\max}
90%	v_x	1.852×10^{-2}	2.361×10^{-1}	1.315×10^{-2}	1.583×10^{-1}
	v_y	8.471×10^{-3}	1.737×10^{-1}	4.582×10^{-3}	7.309×10^{-2}
	ω	3.275×10^{-3}	6.603×10^{-2}	3.098×10^{-3}	5.585×10^{-2}
	L_{\min}	1.48×10^{-4}		6.974×10^{-5}	
60%	v_x	2.181×10^{-2}	2.361×10^{-1}	1.64×10^{-2}	1.583×10^{-1}
	v_y	1.227×10^{-2}	1.737×10^{-1}	8.874×10^{-3}	9.951×10^{-2}
	ω	3.641×10^{-3}	6.37×10^{-2}	3.373×10^{-3}	6.295×10^{-2}
	L_{\min}	2.132×10^{-4}		1.251×10^{-4}	
30%	v_x	2.526×10^{-2}	2.736×10^{-1}	1.95×10^{-2}	1.658×10^{-1}
	v_y	1.469×10^{-2}	1.754×10^{-1}	1.262×10^{-2}	1.269×10^{-1}
	ω	4.753×10^{-3}	6.808×10^{-2}	4.679×10^{-3}	6.707×10^{-2}
	L_{\min}	2.922×10^{-4}		1.889×10^{-4}	
15%	v_x	2.628×10^{-2}	2.577×10^{-1}	2.055×10^{-2}	1.733×10^{-1}
	v_y	1.644×10^{-2}	1.777×10^{-1}	1.378×10^{-2}	1.533×10^{-1}
	ω	5.109×10^{-3}	7.429×10^{-2}	4.553×10^{-3}	7.483×10^{-2}
	L_{\min}	3.29×10^{-4}		2.135×10^{-4}	
5%	v_x	2.795×10^{-2}	3.101×10^{-1}	2.204×10^{-2}	2.135×10^{-1}
	v_y	1.846×10^{-2}	1.799×10^{-1}	1.765×10^{-2}	1.285×10^{-1}
	ω	5.958×10^{-3}	1.293×10^{-1}	4.806×10^{-3}	7.628×10^{-2}
	L_{\min}	3.859×10^{-4}		2.773×10^{-4}	

experiments, each configuration represents the DDM model with the original dataset and the FTHD model with the filtered dataset.

V. CONCLUSION

In this paper, we introduce FTHD, a novel fine-tuning PINN model that integrates hybrid loss functions to enhance vehicle dynamics estimation. FTHD builds upon pre-trained DDM

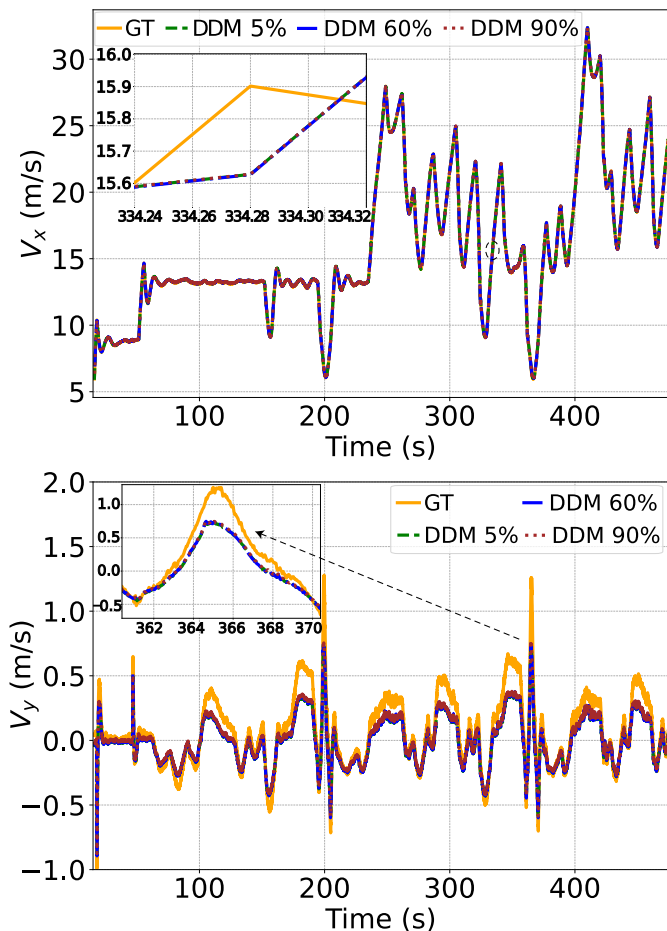


Fig. 11. Velocity prediction of DDM in real experiments as the training set size decreases. (inset) The zoomed-in view highlights the maximum error compared to the GT at the time marked using black dashed circles or lines in the figures.

TABLE VIII

HYPERPARAMETERS USED IN SIMULATION EXPERIMENTS FOR DDM AND FTTHD MODELS, SHOWING CONFIGURATIONS WHERE THE LOWEST VALIDATION LOSS OCCURS AS THE TRAINING DATASET SIZE DECREASES

$\frac{D_{\text{train}}}{D_{\text{sim}}}$	Hidden Layers	Learning Rate	GRU Layers	Hidden Layer size	History timesteps	Batch size
80%	8	0.002510	3	49	9	32
50%	6	0.000734	4	230	7	32
30%	7	0.000898	3	164	3	32
20%	8	0.000985	0	88	18	32
15%	5	0.003907	1	25	18	32

models, providing an innovative framework that leverages both data-driven and differential loss functions to refine vehicle dynamic coefficient estimation. By addressing the limitations of the sigmoid guard layer with fine-tuning and unsupervised differential loss, FTTHD effectively overcomes issues such as local minima, especially with smaller training datasets. The combination of supervised data-driven loss and unsupervised differential loss allows FTTHD to consistently outperform DDM in force estimation, particularly as training data size decreases, leading to reduced validation losses and smaller absolute dif-

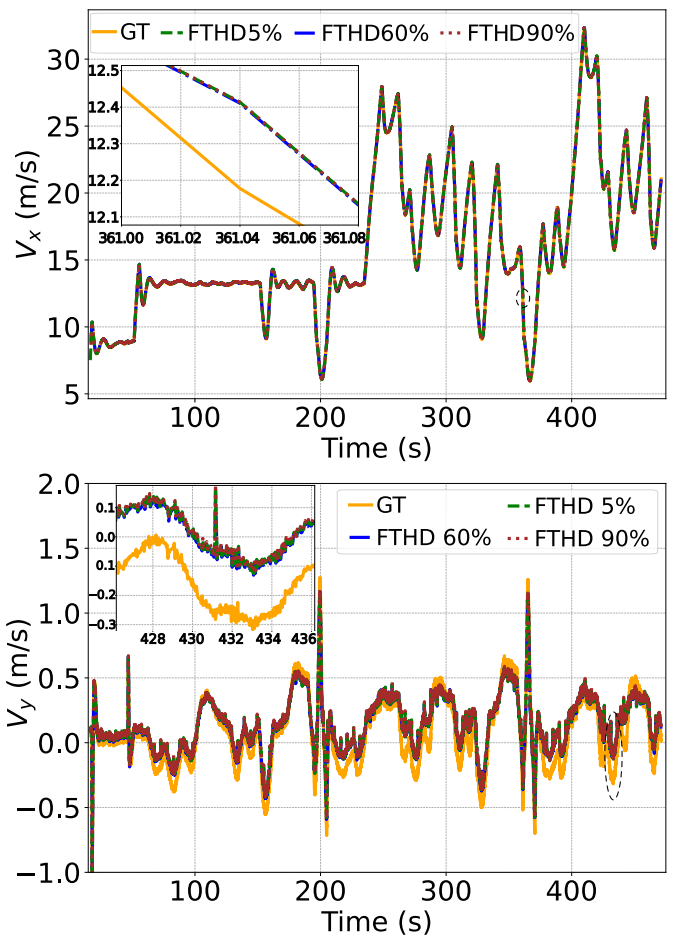


Fig. 12. Velocity prediction of FTTHD in real experiments as the training set size decreases. (inset) The zoomed-in view highlights the maximum error compared to the GT at the time marked using black dashed circles in the figures. FTTHD model demonstrates better overall accuracy in prediction.

TABLE IX

HYPERPARAMETERS USED IN REAL-WORLD EXPERIMENTS FOR DDM AND FTTHD MODELS, INDICATING CONFIGURATIONS WHERE THE LOWEST VALIDATION LOSS OCCURS AS THE TRAINING DATASET SIZE DECREASES

Training Set Ratio	Hidden Layers	Learning Rate	GRU Layers	Hidden Layer size	History timesteps	Batch size
90%	4	0.001378	2	146	16	64
60%	2	0.008942	3	147	18	128
30%	4	0.001904	1	233	10	64
15%	3	0.002941	2	208	14	64
5%	6	0.004099	0	128	4	128

ferences between estimated dynamics parameters and ground truth. Additionally, we propose EKF-FTTHD, a model that integrates an EKF to preprocess noisy real-world data while preserving essential physical relationships between states and controls. EKF-FTTHD addresses the challenge of unknown ground truth vehicle parameters and ranges, allowing the filtered data to improve model performance even in DDM. The results demonstrate that FTTHD offers significant improvements in accuracy and stability when estimating vehicle dynamics, particularly in scenarios with limited training data, making it

a robust solution for real-world applications.

Future research will focus on two key areas. First, expanding the EKF-FTHD approach from the bicycle model to more complex systems, such as four-wheel vehicle models, could improve accuracy and applicability by better addressing real-world measurement errors. This method could also be adapted for other dynamic systems beyond vehicle dynamics, including submarines or agricultural machinery, where estimating internal parameters is challenging. Second, integrating FTHD into the design of distributionally robust control systems could enhance controller performance under uncertainty. By using the noise separated by EKF-FTHD as part of an ambiguity model and eventually incorporating it into the constraints, this approach could advance the development of distributionally robust optimization (DRO) controllers that effectively manage uncertainty and deliver robust performance under varying conditions.

REFERENCES

- [1] E. Bakker, H. B. Pacejka, and L. Lidner, "A new tire model with an application in vehicle dynamics studies," *SAE Trans.*, vol. 98, no. 6, pp. 101–113, 1989.
- [2] T. Weiss and M. Behl, "DeepRacing: A framework for autonomous racing," Grenoble, France, 2020, pp. 1163–1168.
- [3] T. Kim, H. Lee, and W. Lee, "Physics embedded neural network vehicle model and applications in risk-aware autonomous driving using latent features," in *Proc. IEEE/RSJ Int. Conf. Intell. Robot. Syst.*, Kyoto, Japan, 2022, pp. 4182–4189.
- [4] J. Chrosniak, J. Ning, and M. Behl, "Deep dynamics: Vehicle dynamics modeling with a physics-constrained neural network for autonomous racing," *IEEE Robot. Autom. Lett.*, vol. 9, no. 5, pp. 5292–5297, 2024.
- [5] S. Fang and K. Yu, "Fine-tuning hybrid physics-informed neural networks for vehicle dynamics model estimation," in *Proc. Modeling Estimation Control Conf.*, Chicago, IL, USA, 2024, to appear.
- [6] B. A. H. Vicente, S. S. James, and S. R. Anderson, "Linear system identification versus physical modeling of lateral–longitudinal vehicle dynamics," *IEEE Trans. Contr. Syst. Technol.*, vol. 29, no. 3, pp. 1380–1387, 2020.
- [7] J. E. A. Dias, G. A. S. Pereira, and R. M. Palhares, "Longitudinal model identification and velocity control of an autonomous car," *IEEE Trans. Intell. Transport. Syst.*, vol. 16, no. 2, pp. 776–786, 2014.
- [8] C. P. Vyasrayani, T. Uchida, A. Carvalho, and J. McPhee, "Parameter identification in dynamic systems using the homotopy optimization approach," *Multibody Syst. Dyn.*, vol. 26, pp. 411–424, 2011.
- [9] A. Jain and M. Morari, "Computing the racing line using Bayesian optimization," in *Proc. IEEE Conf. Decision Control*, Jeju Island, Republic of Korea, 2020, pp. 6192–6197.
- [10] J. Kabzan, L. Hewing, A. Liniger, and M. N. Zeilinger, "Learning-based model predictive control for autonomous racing," *IEEE Robot. Autom. Lett.*, vol. 4, no. 4, pp. 3363–3370, 2019.
- [11] N. A. Spielberg, M. Brown, N. R. Kapania, J. C. Kegelmann, and J. C. Gerdes, "Neural network vehicle models for high-performance automated driving," vol. 4, no. 28, p. eaaw1975, 2019.
- [12] G. Williams, N. Wagener, B. Goldfain, P. Drews, J. M. Reh, B. Boots, and E. A. Theodorou, "Information theoretic mpc for model-based reinforcement learning," in *Proc. IEEE Int. Conf. Robot. Autom.*, Singapore, 2017, pp. 1714–1721.
- [13] L. Hermansdorfer, R. Trauth, J. Betz, and M. Lienkamp, "End-to-end neural network for vehicle dynamics modeling," Agadir, Morocco, 2021, pp. 407–412.
- [14] P.-F. Xu, C.-B. Han, H.-X. Cheng, C. Cheng, and T. Ge, "A physics-informed neural network for the prediction of unmanned surface vehicle dynamics," vol. 10, no. 2, p. 148, 2022.
- [15] K. Koysuren, A. F. Keles, and M. Cakmakci, "Online parameter estimation using physics-informed deep learning for vehicle stability algorithms," in *Proc. Amer. Control Conf.*, Denver, CO, USA, 2023, pp. 466–471.
- [16] R. W. Schafer, "What is a savitzky-golay filter?[lecture notes]," *IEEE Signal Process. Mag.*, vol. 28, no. 4, pp. 111–117, 2011.
- [17] M. I. Ribeiro, "Kalman and extended kalman filters: Concept, derivation and properties," *Institute for Systems and Robotics*, vol. 43, no. 46, pp. 3736–3741, 2004.
- [18] A. Wischnewski, M. Geisslinger, J. Betz, *et al.*, "Indy autonomous challenge - autonomous race cars at the handling limits," in *Proc. Int. Munich Chassis Symp.*, Munich, Germany, 2022, pp. 163–182.
- [19] M. O'Kelly, V. Sukhil, H. Abbas, *et al.*, "F1/10: An open-source autonomous cyber-physical platform," *arXiv:1901.08567*, www.arxiv.org, 2019.
- [20] H. B. Pacejka and E. Bakker, "The magic formula tyre model," *Vehicle system dynamics*, vol. 21, no. S1, pp. 1–18, 1992.
- [21] D. Liu and Y. Wang, "A dual-dimer method for training physics-constrained neural networks with minimax architecture," *Neural Netw.*, vol. 136, pp. 112–125, 2021.
- [22] C. Lew, "Physics informed neural networks: Reducing data size requirements via hybrid learning," Vancouver, WA, USA, 2022, pp. 178–179.
- [23] G. Swirszcz, W. M. Czarnecki, and R. Pascanu, "Local minima in training of neural networks," *arXiv:1611.06310*, www.arxiv.org, 2016.
- [24] A. Kulkarni, J. Chrosniak, E. Ducote, F. Sauerbeck, A. Saba, U. Chirimar, J. Link, M. Behl, and M. Cellina, "Racecar-the dataset for high-speed autonomous racing," in *Proc. IEEE/RSJ Int. Conf. Intell. Robot. Syst.*, Detroit, MI, USA., 2023, pp. 11 458–11 463.
- [25] R. Liaw, E. Liang, R. Nishihara, P. Moritz, J. E. Gonzalez, and I. Stoica, "Tune: A research platform for distributed model selection and training," *arXiv:1807.05118*, www.arxiv.org, 2018.



Shiming Fang (Student Member, IEEE) received the B.S. degree in Mechanical Engineering from Wuhan University of Technology, Wuhan, China in 2016, and the M.S. degree in Mechanical Engineering from University of Birmingham, Birmingham, UK in 2017. He is currently working towards a Ph.D. degree in Mechanical Engineering at Binghamton University. His current research focuses on autonomous vehicle modeling, robust control, and artificial intelligence in autonomous driving.



Kaiyan Yu (Member, IEEE) received the B.S. degree in intelligent science and technology from Nankai University, Tianjin, China, in 2010, and the Ph.D. degree in mechanical and aerospace engineering from Rutgers University, Piscataway, NJ, USA, in 2017. She joined the Department of Mechanical Engineering, Binghamton University, Binghamton, NY, USA, in 2018, where she is currently an Assistant Professor. Her current research interests include autonomous robotic systems, motion planning and control, mechatronics, automation science and engineering with applications to nano/micro particles control and manipulation, Lab-on-a-chip, and biomedical systems.

Dr. Yu is a member of the American Society of Mechanical Engineers (ASME). She is a recipient of the 2022 US NSF CAREER Award. She currently serves as an Associate Vice President of the *IEEE Robotics and Automation Society (RAS) Media Services Board* (since 2019) and an Associate Editor of the *IEEE TRANSACTIONS ON AUTOMATION SCIENCE AND ENGINEERING*, *IEEE Robotics and Automation Letters*, *IFAC Mechatronics*, *Frontiers in Robotics and AI*, and the *IEEE Robotics and Automation Society Conference Editorial Board* and the *ASME Dynamic Systems and Control Division Conference Editorial Board* (since 2018).